Available online at www.sciencedirect.com
SCIENCE DIRECT®
PERGAMON
Continental Shelf Research 23 (2003) 435–456
CONTINENTAL SHELF RESEARCH
www.elsevier.com/locate/csr

Weak wind-wave/tide interaction over a moveable bottom: results of numerical experiments in Cádiz Bay

B.A. Kagan[a,b], O. Álvarez[a,c,*], A. Izquierdo[a], R. Mañanes[a], B. Tejedor[a], L. Tejedor[a]

[a] *Departamento de Física Aplicada, Universidad de Cádiz, Apdo. 40, 11510 Puerto Real (Cádiz), Spain*
[b] *Shirshov Institute of Oceanology, Russian Academy of Sciences, St. Petersburg Branch, 30 Pervaya Liniya, St. Petersburg 199053, Russia*
[c] *Unidad asociada de Oceanografía interdisciplinar UCA-CSIC, Universidad de Cádiz, Apdo. 40, 11510 Puerto Real (Cádiz), Spain*

Received 4 June 2002; accepted 6 December 2002

Abstract

The formulation of weak wind-wave/low-frequency current interaction is extended to the moveable rough bottom case using the bottom roughness predictors of Nielsen (Coastal Eng. 7 (1983) 233) and Tolman (J. Phys. Oceanogr. 24 (1994) 994). This "extended" formulation is then implemented in a 2D non-linear, high-resolution hydrodynamic model and the modified model is applied to study the changes in the tidal dynamics of Cádiz Bay due to wind-wave/tide interaction and bottom mobility. It is shown that an agreement between the observed and predicted tidal elevation amplitudes and phases at the tide-gauge and bottom-pressure measurement locations within the bay tend to be improved if both of these factors are accounted for. Distinctions between the solutions derived when employing Nielsen's and Tolman's bottom roughness predictors are considerable though not so much as might be expected. The sensitivity of the solution to the mean sediment grain size turns out to be either moderate or low depending on which of the above-mentioned bottom roughness predictors is adopted and much less than the sensitivity to the tidal reference bottom roughness length. Accordingly, if the wave and tidal reference bottom roughness lengths are set equal to each other, the changes in the fields of tidal characteristics become unreasonable, thereby eliminating the possibility of prescribing a single reference bottom roughness length.

Keywords: Weak wave–tide interaction; Bottom mobility

1. Introduction

The interaction between wind waves and tides goes on independent of whether or not sediment motion and its related changes in dimension, shape and mutual arrangement of bottom roughness elements occur. For brevity, the process of changing these bottom roughness elements will be referred to as "bottom mobility". With no bottom mobility (the case of a fixed bottom), wind-wave/tide interaction is caused by immediate linear or non-linear superposition of the individual wave and tidal bottom stresses. Because of this the

*Corresponding author. Department of Applied Physics, Faculty of Marine Sciences, University of Cádiz, Apt. 40, Puerto Real (Cádiz), Spain. Tel./fax: +34-956-01-6079.
E-mail address: oscar.alvarez@uca.es (O. Álvarez).

0278-4343/03/$ - see front matter
doi:10.1016/S0278-4343(02)00223-6

drag coefficient and energy dissipation increase in the near-bottom layer, tending to modify wave and tidal dynamics. With bottom mobility (the case of a moveable bottom), the events can begin with and/or be accompanied by wave- and tide-induced changes in bottom roughness capable of altering both the intermediate and end consequences of wind-wave/tide interaction. These changes in bottom roughness can be accompanied by changes in suspended sediment concentration and sediment stratification. The latter along with the changes in bottom roughness will modify near-bottom turbulence and, hence, flow characteristics. We shall try to assess the first of the above-mentioned factors. The influence of sediment stratification on tidal dynamics has been evaluated in particular in Álvarez et al. (1999) and Kagan et al. (2003). A detailed discussion of changes in the three-dimensional (3D) structure of tidal flow due to wind-wave forcing may be found in Davies and Lawrence (1994) and Davies and Jones (1996).

At present, there are two formulations of wind-wave/low-frequency current interaction. One of them proposed by Grant and Madsen (1979) assumes that wave and low-frequency components of bottom stress are influenced by each other and are enhanced in the process of their interaction. As a result, the total bottom friction velocity differs from the sum of wave and low-frequency bottom friction velocities. The interaction of this type is said to be strong. This formulation was somewhat modified by Christofferesen and Jonsson (1985) and Signell et al. (1990). In particular, Signell et al. (1990) suggested that the low-frequency current affected the wave bottom stress only if the wave bottom stress was a minor fraction of the total bottom stress. It followed that there was a certain need for revision of the concept of strong wind-wave/low-frequency current interaction. In this context it is not out of place to cite a remark of a reviewer of this paper who, based on results of reanalysis of existing data, concluded that there was neither theoretical nor experimental evidence of a strong impact of mean currents on the wave stress, even in the "strong interaction" approach.

Another formulation of weak wind-wave/low-frequency current interaction (Kagan and Utkin, 2000; Kagan et al., 2001) starts from the belief that the interaction between motions with widely different spatial and temporal scales can be weak, even though these motions are in themselves strongly non-linear. This is tantamount to that the bottom friction velocities with wave and low frequencies are weakly correlated and that, hence, their linear superposition provides an adequate description of the total bottom friction velocity in a combined motion of wind waves and low-frequency currents.

Both of these formulations are satisfactory consistent with the CODE-1 and CODE-2 data (Grant et al., 1984), which is not surprising taking into account a wide scatter in the data. The scatter may be connected, among other things, with bottom mobility which role, like the role of its associated changes in low-frequency flow dynamics, remains poorly understood. To the authors' knowledge, the only work that is relevant to the problem under study is the work of Davies and Lawrence (1995). It shows that a spatially variable bottom roughness reflecting the range of the bottom composition, not bottom mobility, in the eastern Irish Sea could give rise to a slightly different wind-driven circulation when wave–current interaction is accounted for.

By contrast, the transformation of surface gravity waves due to sediment motion has long been the subject of investigation (see, e.g., Graber and Madsen, 1988; Tolman, 1994, 1995; Young and Gorman, 1995; Johnson and Kofoed-Hansen, 2000; Ardhuin et al., 2001). It has been apparent in the papers listed that, in the absence of strong local forcing, sediment motion has a profound impact on the evolution of wave spectra, especially on swell propagation in shallow waters.

Out of all currently available bottom roughness predictors, two most popular predictors in the wind-wave modelling community are those proposed by Nielsen (1983) and Grant and Madsen (1982), the latter being usually adopted in the modified version of Tolman (1994). These are based on laboratory data mainly for monochromatic waves and rely upon much of similar assumptions. Namely, depending on the value of the Shields parameter (the ratio squared of the wave skin friction velocity to the settling velocity of suspended sediment particles), the bottom

roughness is considered to be in one of three regimes. The first of them occurs when wave motion is too weak to cause sediment motion and the bottom roughness is taken as a reference one (a sediment grain bottom roughness, after Nielsen (1983), and a background bottom roughness, after Tolman, 1994). As soon as the Shields parameter becomes larger than its critical value for initial sediment motion, ripples begin to form. Accordingly, the bottom roughness increases by a jump to the ripple roughness. As the Shields parameter continues to increase, ripples, upon attaining an equilibrium state, wash out gradually, resulting in a decrease in the bottom roughness. The decay of ripples is accompanied by the development of a sheet flow (the flow of highly concentrated rolling, saltating and suspended sediment particles in the thin near-bottom layer) and the bottom roughness is identified with the sheet-flow roughness.

Now, if expressions for the ripple and sheet-flow bottom roughness lengths are known, then an expression for the bottom roughness in the general case, which encompasses all sediment motion regimes, may be obtained by matching of appropriate asymptotes. It is such an expression that serves as a bottom roughness predictor. Testing some of available predictors in field conditions, Li and Amos (1998) inferred that the predictors of Nielsen (1983) and Grant and Madsen (1982) over-estimated the ripple roughness. Wiberg and Rubin (1989) came to the same conclusion as applied to the sheet-flow roughness using unidirectional flume data. Under unidirectional flows, however, the sheet-flow roughness for a given bottom stress is about one order of magnitude less than that under waves (Dietrich, 1982). This suggests that these predictors over-estimate the sheet-flow roughness, as applied to waves, too. The deficiency of available bottom roughness predictors for monochromatic waves, when applied to irregular waves, was first indicated by Madsen et al. (1990) and used explicitly by Tolman (1994).

For lack of a better means we shall make use of Nielsen's (1983) and Tolman's (1994) bottom roughness predictors and a "climatological" wave field to quantify the influence of bottom mobility on the wave-affected tidal flow in Cádiz Bay; to this end, a preliminary refining of the formulation of weak wind-wave/low-frequency current interaction will be carried out to take into account of the bottom mobility effects. Such are the aims of the present paper.

The paper is organised as follows. In Section 2 the formulation of weak wind-wave/tide interaction is extended to the moveable rough bottom case. Section 3 presents a brief description of the region of interest and the 2D non-linear, high-resolution hydrodynamic model in which this "extended" formulation is inserted. Results of the application of the modified model to simulate the M2 tidal dynamics of Cádiz Bay and its changes due to wind-wave/tide interaction and bottom mobility are discussed in Section 4. Section 5 contains the summary of this work and a list of some unresolved problems closely related to the problem considered.

2. Formulation of weak wind-wave/tide interaction in the moveable rough bottom case

In the moveable rough bottom case the weak interaction between wind waves and tides is described by the same equations as in Kagan and Utkin (2000) and Kagan et al. (2001), with the only difference that the hydrodynamic bottom roughness length is determined through one or another of the bottom roughness predictors. This modified formulation involves the relation for the drag coefficient, c_D, in tidal flow which, with due regard for bottom mobility, is specified as

$$c_D^{-1/2} = c_{D0}^{-1/2} - \frac{1}{\kappa}\Big[\ln(1+\gamma) + \gamma(1+\gamma)^{-1} \times \ln\left(\frac{\delta_w}{z^r_{ow}}\right)\left(\frac{z^r_{ow}}{z^r_{oT}}\right) + (1+\gamma)^{-1}\ln\left(1+m\frac{z^r_{ow}}{z^r_{oT}}\right) - \ln\left(1+\gamma\left(\frac{\delta_w}{z^r_{ow}}\right)\left(\frac{z^r_{ow}}{z^r_{oT}}\right)\exp(-\kappa c_{D0}^{-1/2})\right)\Big], \quad (1)$$

the ratio, γ, between wave and tidal bottom friction velocity amplitudes (U_{*w} and U_{*T}, respectively)

$$\gamma = \frac{U_{*w}}{U_{*T}}, \quad (2)$$

the relations for the scaled wave and tidal bottom boundary layer (BBL) depths (δ_w/z^r_{ow} and δ_T/z^r_{oT},

respectively)

$$\frac{\delta_w}{z^r_{ow}} = \kappa \frac{U_{*w}}{U_{w\infty}} Ro^r_w, \tag{3}$$

$$\frac{\delta_T}{z^r_{oT}} = \kappa \frac{U_{*T}}{U_{T\infty}} Ro^r_T, \tag{4}$$

the surface Rossby number dependences for the wave and tidal bottom friction coefficients ($U_{*w}/U_{w\infty}$ and $U_{*T}/U_{T\infty}$, respectively) inferred from the resistance law for an oscillatory rough turbulent BBL

$$\left[(2.3A)^2 + \left(2.3B + \ln 2^{-5/2}\kappa + \frac{\kappa U_{w\infty}}{U_{*w}}\right)^2\right]^{1/2} = \ln Ro^r_w - \ln \frac{U_{w\infty}}{U_{*w}} + \ln \kappa - \ln(1+m), \tag{5}$$

$$\left[(2.3A)^2 + \left(2.3B + \ln 2^{-5/2}\kappa + \frac{\kappa U_{T\infty}}{U_{*T}}\right)^2\right]^{1/2} = \begin{cases} \left(\ln Ro^r_T - \ln \dfrac{U_{T\infty}}{U_{*T}} + \ln \kappa - \ln\left(1 + m\dfrac{z^r_{ow}}{z^r_{oT}}\right)\right) & \text{if } \delta_T < h, \\ \ln \dfrac{h}{z^r_{oT}} - \ln\left(1 + m\dfrac{z^r_{ow}}{z^r_{oT}}\right) & \text{if } \delta_T \geqslant h, \end{cases} \tag{6}$$

the expression for the sediment mobility parameter, m, which is defined as the ratio of wave-induced changes in the bottom roughness length to the wave reference bottom roughness length and which, in terms of the wave surface Rossby number, is written as

$$m = \begin{cases} 0 & \text{if } \dfrac{\theta'}{\theta'_c} < 1, \\ 1.90(Ro^r_w)^{-2.7}\left(\sigma_w\sqrt{\dfrac{d}{g'}}\right)^{-3.7}\left(1 - 0.47\left(\dfrac{\theta'}{\theta'_c}\right)^{-1/4}\right)\left(\dfrac{d}{z^r_{ow}}\right)^{3.7} + 1.42\left(\dfrac{\theta'}{\theta'_c} - 1\right)^{1/2}\dfrac{d}{z^r_{ow}} & \text{if } 1 \leqslant \dfrac{\theta'}{\theta'_c} \leqslant 20, \\ 1.42\left(\dfrac{\theta'}{\theta'_c} - 1\right)^{1/2}\dfrac{d}{z^r_{ow}} & \text{if } \dfrac{\theta'}{\theta'_c} > 20, \end{cases} \tag{7a}$$

by Nielsen (1983), and

$$m = \begin{cases} 0 & \text{if } \dfrac{\theta'}{\theta'_c} < 1.2, \\ 0.05 Ro^r_w \left(\dfrac{\theta'}{\theta'_c}\right)^{-2.5} + 0.218 \times 10^{-2}\left(Ro^r_w\right)^{2.4}\left(\sigma_w\sqrt{\dfrac{d}{g'}}\right)^{2.8}\left(\dfrac{d}{z^r_{ow}}\right)^{-1.4} & \text{if } \dfrac{\theta'}{\theta'_c} \geqslant 1.2, \end{cases} \tag{7b}$$

by Tolman (1994), and the definition of the Shields parameter, θ', expressed in terms of the wave surface Rossby number as

$$\theta' = \left(\frac{U'_{*w}}{U_{w\infty}}\right)^2 (Ro'_w)^2 \left(\sigma_w\sqrt{\frac{d}{g'}}\right)^2 \left(\frac{d}{z'_{ow}}\right)^{-2}. \tag{8}$$

Here, except for already known designations, $Ro^r_w = U_{w\infty}/\sigma_w z^r_{ow}$ and $Ro'_w = U_{w\infty}/\sigma_w z'_{ow}$ are the wave surface Rossby numbers based on z^r_{ow} and z'_{ow}, respectively; $Ro^r_T = U_{T\infty}/\sigma_T z^r_{oT}$ is the tidal surface Rossby number; $U_{w\infty}$ and σ_w are the rms wave near-bottom orbital velocity amplitude and the spectrally averaged wave frequency specified, to the quasi-monochromatic approximation of the wave field, as

(Longuet-Higgins, 1969).

$$U_{w\infty} = \left(2\int_0^\infty S_u(\sigma,h)\,\mathrm{d}\sigma\right)^{1/2}, \tag{9}$$

$$\sigma_w = \int_0^\infty \sigma S_u(\sigma,h)\,\mathrm{d}\sigma \Big/ \int_0^\infty S_u(\sigma,h)\,\mathrm{d}\sigma, \tag{10}$$

$S_u(\sigma,h)$ is the wave near-bottom orbital velocity spectrum related to the depth-limited wave spectrum, $S(\sigma,h)$, by the relationship $S_u(\sigma,h) = \sigma^2 S(\sigma,h)/\sinh^2 kh$; σ and k are the spectral wave frequency and wave number related to one another by the dispersion relation $\sigma^2 = gk\tanh kh$ for linear waves in shallow waters; $U_{T\infty}$ is the friction-free tidal velocity amplitude; σ_T is the tidal frequency; h is the local water depth; z^r_{ow} and z^r_{oT} are the wave and tidal reference bottom roughness lengths, the former of which being prescribed as $z^r_{ow} = d/12$ in the bottom roughness predictor of Nielsen (1983) and $z^r_{ow} = 0.03$ cm (or 1/30 of a Nikuradse roughness of 1 cm) in the bottom roughness predictor of Tolman (1994); U'_{*w} is the skin friction velocity amplitude defined as $U'_{*w} = U_{*w}$ at $z^r_{ow} = z'_{ow}$; z'_{ow} is the sediment grain roughness length specified as $z'_{ow} = d/12$, after Nielsen (1983), and $z'_{ow} = d/30$, after Tolman (1994); θ'_c is the critical Shields parameter for the initiation of sediment motion; d is the mean sediment grain size; $c_{D0} = \kappa^2/\ln^2(z_1/z^r_{oT})$ is the reference drag coefficient in tidal flow over a fixed bottom; z_1 is a reference height within the near-bottom logarithmic layer but above the wave BBL; $g' = g(\rho_S - \rho_w)/\rho_w$ is reduced gravity; ρ_S and ρ_w are sediment and water densities; g is the acceleration due to gravity; $A = 0.92$ and $B = 1.38$ are numerical constants; $\kappa = 0.4$ is von Karman's constant.

The assumptions underlying Eqs. (1)–(10) are as follows: (i) the total bottom friction velocity in a combined motion of wind waves and tides is defined as the sum of the individual wave and tidal bottom friction velocities; (ii) the vertical eddy viscosity is a function of the total bottom friction velocity in the wave BBL and the tidal bottom friction velocity above the wave BBL; (iii) the wave and tidal bottom friction coefficients are determined by the common resistance law for an oscillatory rough turbulent BBL with different values of the external parameters; (iv) it is believed that, because the wave time scale is much less than the tidal time scale and, hence, the wave BBL depth is much less than the tidal BBL depth, the vertical wave orbital velocity shear and the wave bottom stress in the wave BBL are much larger than their tidal analogues in the tidal BBL; (v) if so, the changes in the bottom roughness length are wave-dominant; (vi) the time scale of the ripple generation is much less than the time scale of the evolution of the wave field, resulting in jump-like changes in the bottom roughness length; and (vii) the random wave field is described within the framework of the quasi-monochromatic approximation.

Only certain of these assumptions have been supported by observational evidence; the others, for lack of experimental data, are based on pure qualitative considerations. Nevertheless, when taken together, they allow us to develop a comparatively simple and, as we would like to hope, physically sound means for quantifying the effects of wind-wave/tide interaction over a moveable rough bottom in terms of the drag coefficient in tidal flow. From Eqs. (1)–(7) we notice that, if both of the factors, wind-wave/tide interaction and bottom mobility, are concurrently accounted for, the drag coefficient is determined by six dimensionless combinations of the external parameters, Ro^r_w, Ro^r_T, $U_{w\infty}/U_{T\infty}$, $\sigma_w(d/g')^{1/2}$, d/z^r_{ow} and d/z^r_{oT}, when employing the bottom roughness predictor of Tolman (1994) and by the first five of them when employing the bottom roughness predictor of Nielsen (1983). Here, $\sigma_w(d/g')^{1/2}$ is the ratio of the spectrally averaged (or any one representative) wave frequency σ_w to the buoyancy frequency $(g'/d)^{1/2}$ of suspended particles appearing in the definition of the sediment mobility parameter; the physical interpretation of the remaining combinations is evident. A decline in the number of such combinations is explained by the different choice of the reference bottom roughness length. In fact, if in Tolman's (1994) predictor the above length is assumed to be fixed and equal to a background bottom roughness length, then in Nielsen's (1983) predictor it is taken to be proportional to the mean sediment grain size with a proportionality factor of 1/12. We reserve a

further discussion of this aspect of the problem considered for Sections 4 and 5.

3. Investigation site and model

The above "extended" formulation of weak wind-wave/tide interaction has been applied to Cádiz Bay where detailed tide-gauge and bottom-pressure measurements along the coast and in the interior of the bay have been made during the last few years.

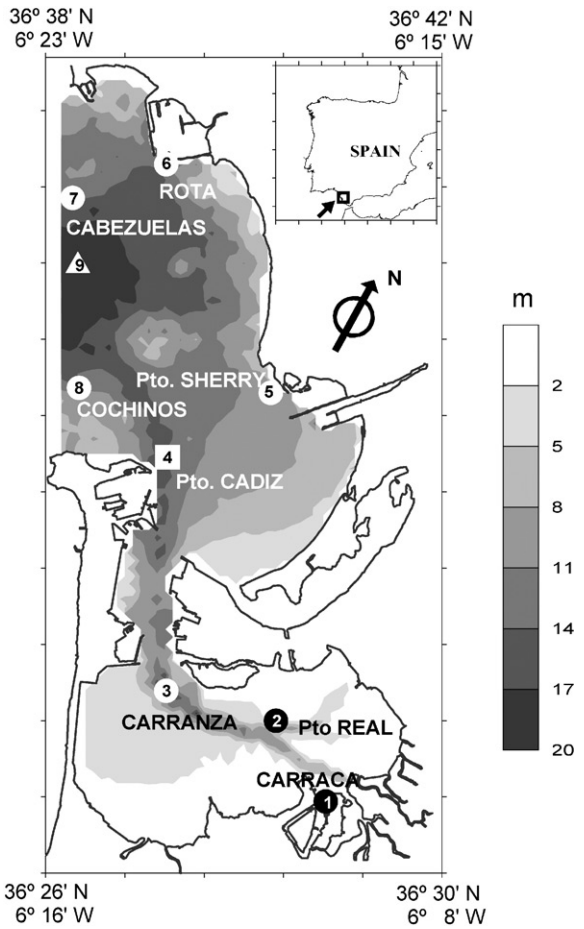

Fig. 1. Map of Cádiz Bay superimposed on the bathymetry (in m). The location of a tide-gauge is denoted by the square; the locations of the bottom-pressure sensors, by open and closed circles; and the location of a current-meter mooring, by the triangle. A general location map is shown in the inset.

Cádiz Bay is near latitude 36.5°N on the southwestern coast of Spain (Fig. 1). It faces west towards the Gulf of Cádiz and is landlocked around its southwestern, southern and eastern margins by the mainland. The bay is subdivided into two parts, the shallower Inner Bay and the deeper Outer Bay, connected by the narrow Puntales Channel. The bay is relatively shallow, with a maximum depth of 20 m at its seaward edge, and is characterised by predominantly semidiurnal co-oscillating tides with an amplitude of $\sim$1 m for the M2 constituent and $\sim$0.4 m for the S2 constituent.

The typical wind waves in the bay are short-period waves with periods below 7 s and amplitudes of $\sim$0.5 m in summer and $\sim$1 m in winter. The shape of wave spectra in the region of interest is similar to that of wave spectra in waters of finite depth. It is characterised by a rather sharp peak and a high-frequency flank with a negative power frequency dependence of the spectral density. The power of frequency on this flank is about -3.5. On a low-frequency flank there is a secondary peak at the frequencies of swell. The periods of swell components are 12–15 s.

Sea-bed sediments in the bay consist mainly of coarse silt with a median grain size of 40 μm and medium sand with a median grain size of 190 μm. Quartz grains comprise 85% of all sediments (Gutiérrez et al., 1996).

The 2D non-linear, high-resolution hydrodynamic model developed by Álvarez et al. (1997) was applied to simulate the response of the M2 tidal dynamics of Cádiz Bay to the impact of wind-wave/tide interaction and bottom mobility. The model is based on the mass-conservation and momentum equations in depth-averaged form. A condition of no-flow normal to the coast was set at the land boundaries. The latter were made coincident with vertical walls at the local water depth 1 m, thereby eliminating the effects of flooding and drying of mud flats from consideration.

At the open boundary, a radiation condition written in terms of deviations of tidal elevation and velocity from their observed values was employed to ensure that, when disturbances were generated, they all propagated away from the

model domain. The observed values of tidal elevation along the open boundary were obtained using a linear interpolation/extrapolation of those derived from the bottom-pressure measurements at stations Cochinos and Bajo de Cabezuelas (see Fig. 1), while the observed values of tidal velocity were taken as being equal to the M2 tidal velocity from the data at the current-meter mooring location at the open boundary.

Clearly, the observed values of tidal elevation and velocity at the open boundary carry information on wind-wave/tide interaction and bottom mobility inside of the bay. To minimise the influence of these factors on tidal characteristics at the open boundary in the situations when either both or one of them are/is not considered, the appropriate solutions were found in an extended domain covering Cádiz Bay and an adjacent part of the Gulf of Cádiz. In so doing, the open boundary of the extended domain was placed at a depth of 50 m or more where wave-induced changes in the tidal dynamics and the bottom mobility effects became much less than in the bay by itself. The observed values of tidal elevation and velocity at this boundary were identified with the computed ones obtained using a non-linear, high-resolution, boundary-fitted coordinate, curvilinear tidal model of the adjacent part of the Gulf of Cádiz (Tejedor et al., 1998).

For the solution to be smooth the equations of motion were supplemented by a Laplacian horizontal eddy viscosity operator acting on the tidal velocity throughout the model domain except for its boundaries. The horizontal eddy viscosity was kept, from pure computational considerations, to a minimum of $1\,m^2\,s^{-1}$ to suppress short-wavelength numerical disturbances, but, at the same time, to avoid excessively strong smoothing of the derived solution.

The rms near-bottom wave orbital velocity amplitude and the spectrally averaged wave frequency were obtained using the known typical wave spectrum and local depths. In the shallows where local depths were less than twice the rms wave amplitude, the wave amplitude was assumed to be depth-limited due to wave breaking and equal to half of the local water depth. This condition is identical with the empirical wave-breaking criterion adopted by Tang and Grimshaw (1996). It is clear that the typical wave spectrum is of limited application. A discussion of its associated potential deficiencies, however, is beyond the scope of our paper.

The bottom stress related to the depth-averaged tidal velocity was parameterised using a quadratic resistance law with the drag coefficient taken as previously described in order to account for the effects of wind-wave/tide interaction and bottom mobility. The reference drag coefficient and the tidal reference bottom roughness length were specified as $c_{D0} = 0.003$ and $z^r_{oT} = 0.5$ cm, respectively. The above value of c_{D0} is in approximate agreement with the prescribed value of z^r_{oT} and is based on the reference height 0.5 m above the bottom. Generally, c_{D0} and z^r_{oT} do not remain constant if there are changes in bed type and sediment grain size (Heathershaw, 1981). The assumption of constancy of these quantities, however, is likely to be acceptable approximation for Cádiz Bay where no significant spatial variations in bed type and form occur. A detailed discussion of this subject may be found in the papers of Aldridge and Davies (1993) and Davies and Lawrence (1995).

As an approximate estimate which, nevertheless, falls in the range of the observed values, the mean sediment grain size was taken to be 50 μm. The critical Shields parameter and reduced gravity were prescribed to be 0.05 and $1.65\,10^3\,cm\,s^{-2}$, respectively. The latter of these values is typical of quartz grains. The bathymetry was deduced from the IHM chart number 443.

The model equations were integrated on an Arakawa C staggered grid using a semi-implicit Cranck–Nicolson scheme. A spatial resolution of 210 m and a time step of 30 s were chosen. The model was run for 10 tidal cycles to achieve a stable time-periodic solution. After establishing this solution, the model run was continued for one more tidal period so as to determine the M2 tidal constants of elevation and velocity through a harmonic analysis of the relevant time series. Thereafter the cotidal chart and the maps of tidal velocity ellipse parameters and mean (over a tidal cycle) tidal energy budget characteristics were constructed.

4. Modelling results

The modified tidal model was applied in two series of numerical experiments. One of them is intended to quantify the influence of bottom mobility upon the M2 wave-affected tidal flow in Cádiz Bay. It involves four numerical experiments: a control experiment with none of wind-wave/tide interaction and bottom mobility (a conventional approach), the second one with wind-wave/tide interaction and without bottom mobility (a fixed bottom roughness length), and two subsequent numerical experiments in which, along with wind-wave/tide interaction, allowances are made for bottom mobility by means of the bottom roughness predictors of Nielsen (1983) and Tolman (1994). These numerical experiments are referred to as Experiments 0, 1, 2.1 and 2.2, respectively.

The second series comprises numerical experiments on the sensitivity of the derived solution to the tidal reference bottom roughness length and the mean sediment grain size. These experiments, depending on which of the two bottom roughness predictors is used, are referred to as Experiments 3.1, 3.2, 4.1 and 4.2. In all the experiments, except for the experiment with no waves, the rms near-bottom wave orbital velocity and the spectrally averaged wave frequency were calculated using the typical wave spectrum with an rms amplitude and a spectrally averaged wave period of 0.67 m and 5.7 s, respectively. These values were considered to be invariant throughout the bay, excluding the near-shore shallows where the wave amplitude was taken, as indicated above, to be half the local water depth.

4.1. Influence of wind-wave/tide interaction and bottom mobility upon the M2 tidal dynamics of Cádiz Bay

The modelling results for Experiments 0 and 1 have been described in the paper of Kagan et al. (2001). In the present work Experiment 1 was repeated using the quasi-monochromatic approximation of the wave field instead of the monochromatic approximation adopted previously. When employing these approximations, the results differ only in magnitude, making their detailed analysis unnecessary in this paper.

As before, the interaction between wind waves and tides leads to an increase in the drag coefficient (Fig. 2a) which in the Inner Bay may be as much as 0.021, contrary to 0.003 in the no-wave case. Increasing the drag coefficient causes the mean (over a tidal cycle) bottom stress to rise (Fig. 3b) and the maximum depth-averaged tidal velocity to fall (Fig. 4b) in the Inner Bay. Such high values of c_D in the first case as well as their apparent disagreement with those obtained in the second case are due to a strong sensitivity of Nielsen's (1983) formulation to the wave surface Rossby number (see also Section 5). Their changes amount, by modulus, up to $0.22\,\mathrm{N\,m^{-2}}$ and $2.0\,\mathrm{cm\,s^{-1}}$, respectively. By contrast, in the deeper regions of the Outer Bay the maximum depth-averaged tidal velocity slightly increases due to enhancing the mean tidal energy flux through the open boundary of the bay (Fig. 5b). Here the change in the mean tidal energy flux per unit length reaches its peak of $0.6\,\mathrm{kW\,m^{-1}}$. For a detailed discussion of this point see Kagan et al. (2001). Eventually, the tidal elevation amplitudes and phases and the mean tidal energy dissipation within the bay tend to increase by 0.14 cm, 0.9° and $0.03\,\mathrm{W\,m^{-2}}$, respectively (Figs. 6b, 7b and 8b).

The two factors (wind-wave/tide interaction and bottom mobility) together have a cumulative effect on the tidal dynamics of Cádiz Bay. The mere fact that these factors set up qualitatively the similar changes in tidal characteristics is not surprising. Suffice it to remember that, in accordance with the bottom roughness predictors in use, sediment motion, no matter if it is in the ripple or sheet-flow regime, is responsible exclusively for increasing the bottom roughness length. Because of this, bottom mobility, like wind-wave/tide interaction, entails an increase in the drag coefficient and then all the above-mentioned sequence of events.

The changes in the drag coefficient in Experiments 2.1 and 2.2 may be one order of magnitude more than in Experiment 1 and have closely similar spatial distributions (Figs. 2b and c). As in Experiment 1, the most values of c_D which now amount to as much as 0.35 when using Nielsen's (1983) bottom roughness predictor and 0.069 when

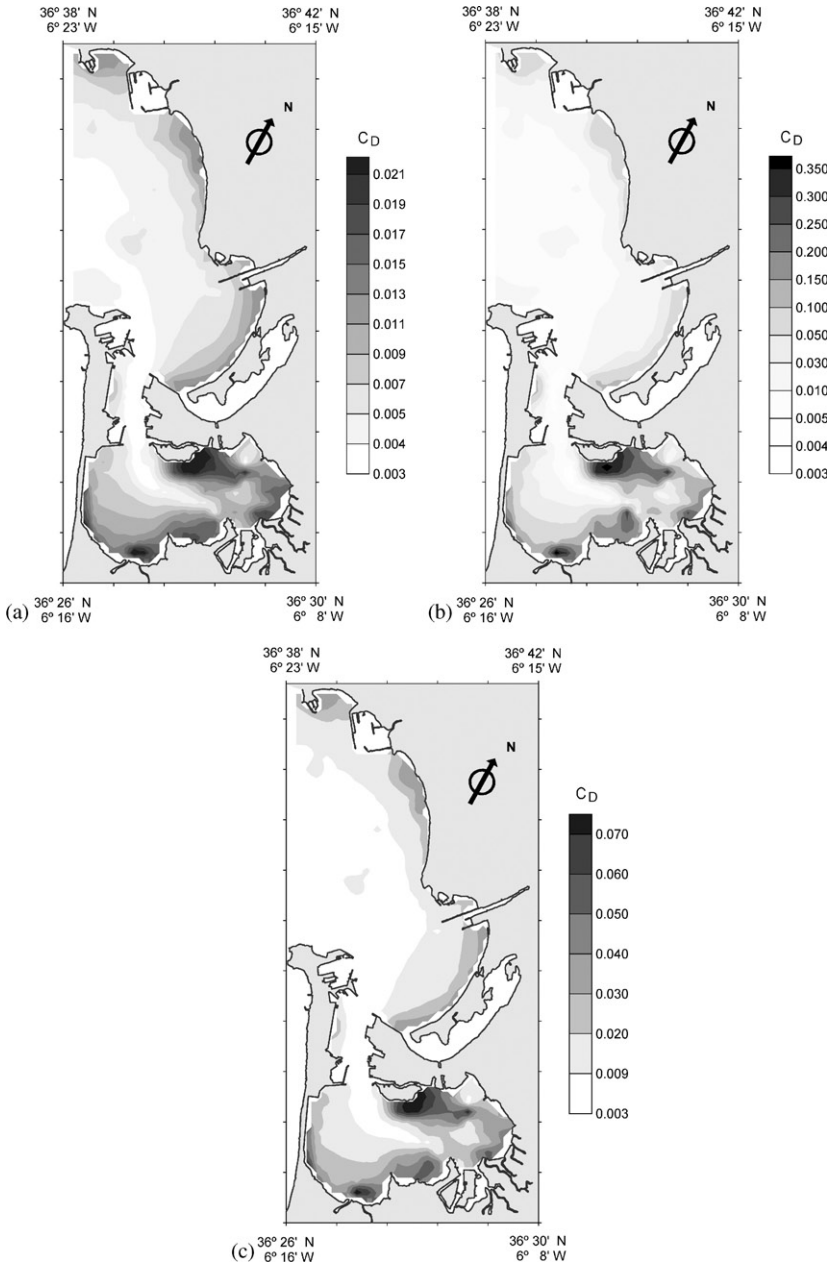

Fig. 2. Drag coefficient obtained with allowance for wind-wave/tide interaction (a) and wind-wave/tide interaction and bottom mobility together (b, c). Results based on Nielsen's (1983) and Tolman's (1994) bottom roughness predictors are presented in the panels (b) and (c), respectively.

using Tolman's (1994) bottom roughness predictor occur in the Inner Bay. Such high values of c_D in the first case as well as their apparent disagreement with those obtained in the second case are due to a strong sensitivity of Nielsen's (1983) predictor to variations of the wave surface Rossby number (see also Section 5). In both the cases the drag coefficient reaches its maximum at the periphery

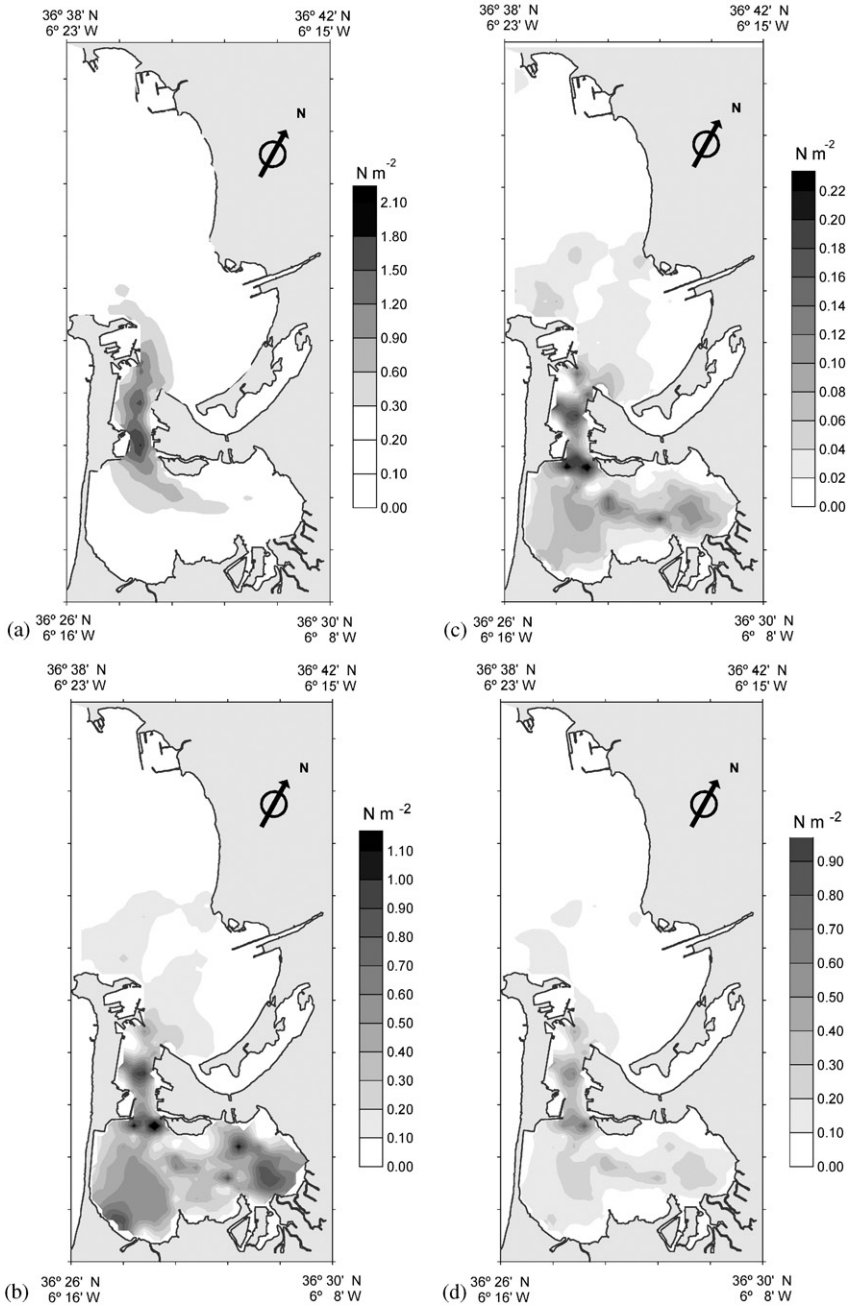

Fig. 3. Bottom stress (a) and its changes caused by wind-wave/tide interaction (b) and wind-wave/tide interaction and bottom mobility together (c, d). Results based on Nielsen's (1983) and Tolman's (1994) bottom roughness predictors are presented in the panels (c) and (d), respectively.

of the Inner Bay, while in the Puntales Channel and the Outer Bay it is basically smaller than 0.005 and exceed this value only in the shallows. As a result, the changes in tidal characteristics in Experiment 2.1 look like and differ from those in Experiment 2.2 in magnitude only (see Figs. 3c,

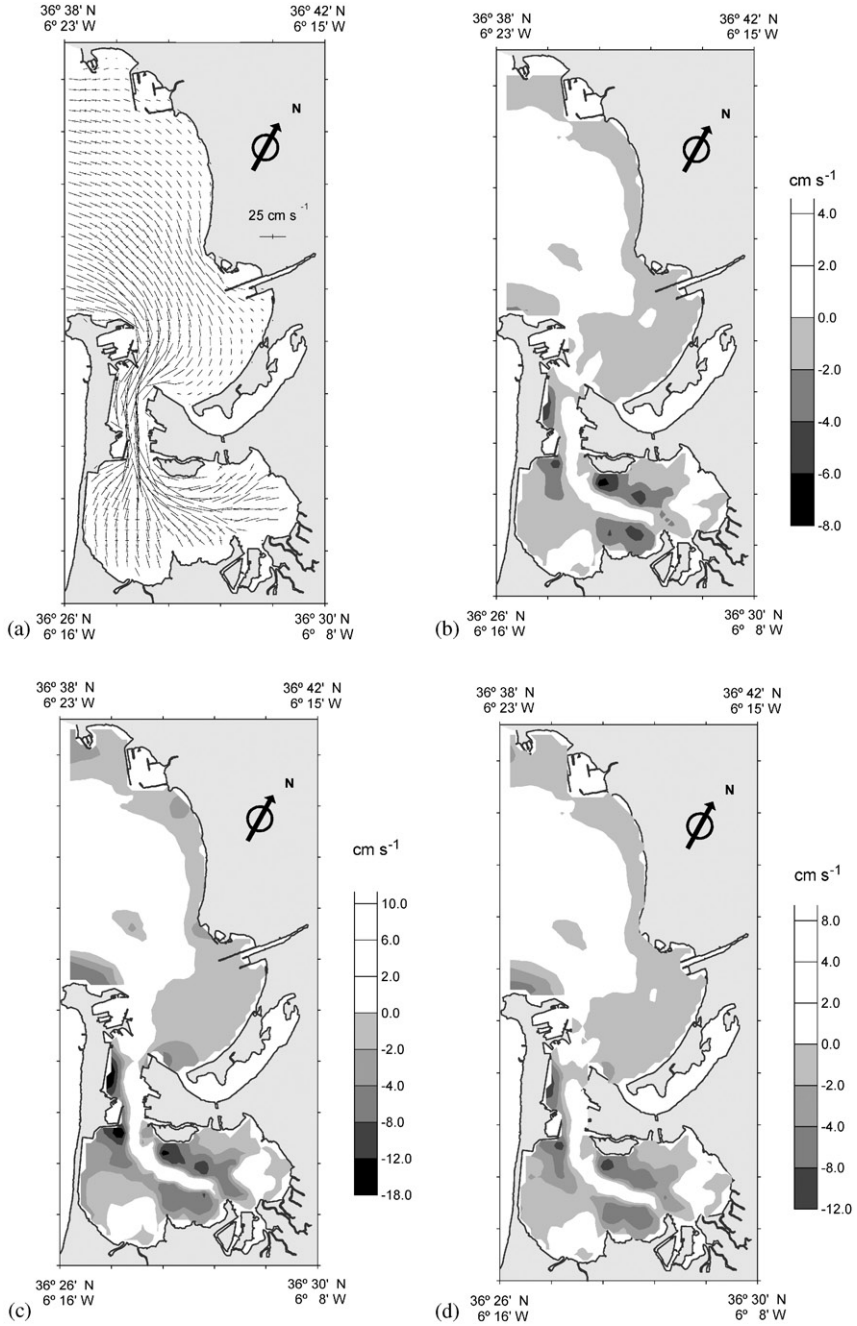

Fig. 4. Major and minor axes of the M2 tidal ellipses (a) and the changes in maximum depth-averaged tidal velocity caused by wind-wave/tide interaction (b) and wind-wave/tide interaction and bottom mobility together (c, d). Results based on Nielsen's (1983) and Tolman's (1994) bottom roughness predictors are presented in the panels (c) and (d), respectively.

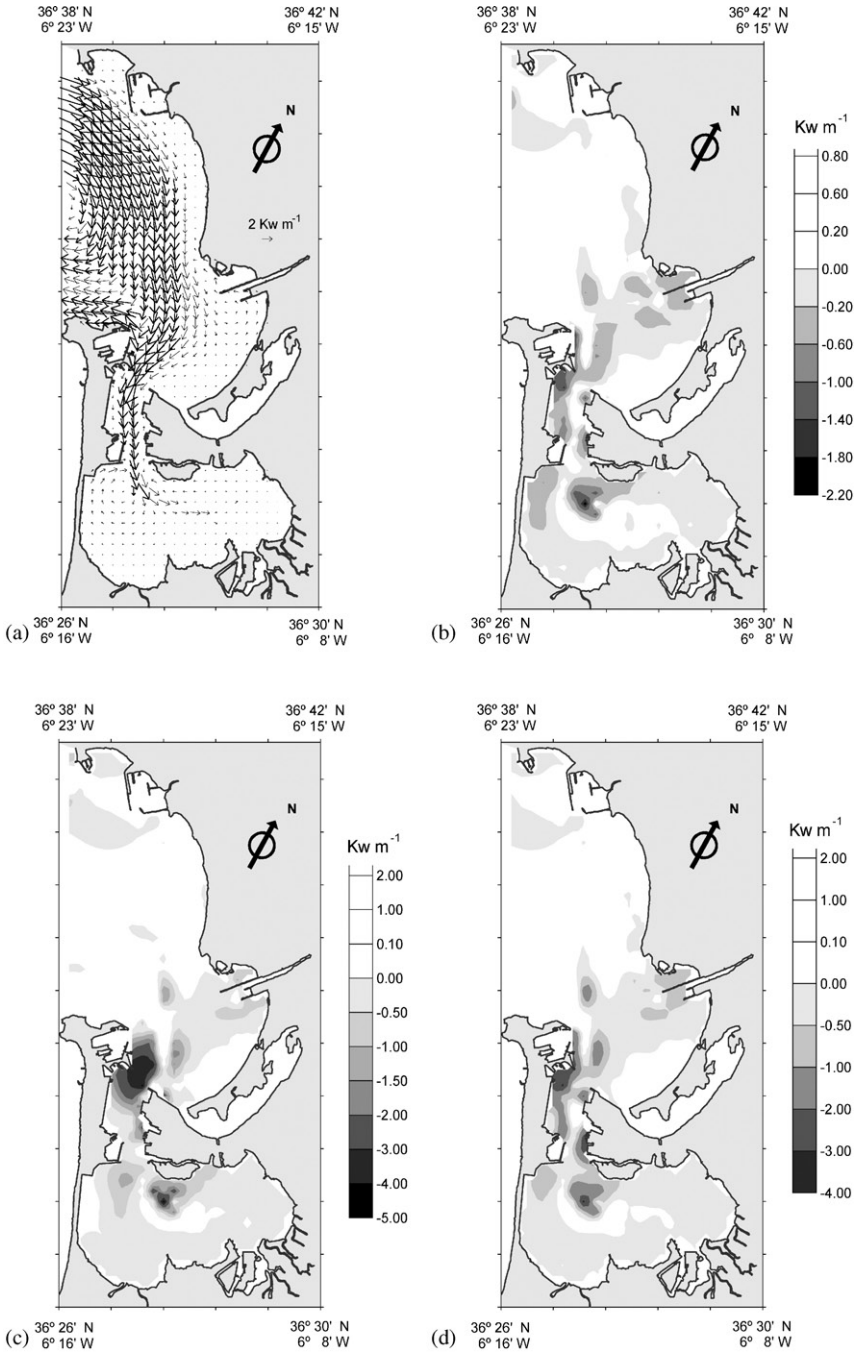

Fig. 5. Mean tidal energy flux per unit length (a) and its changes caused by wind-wave/tide interaction (b) and wind-wave/tide interaction and bottom mobility together (c, d). Results based on Nielsen's (1983) and Tolman's (1994) bottom roughness predictors are presented in the panels (c) and (d), respectively.

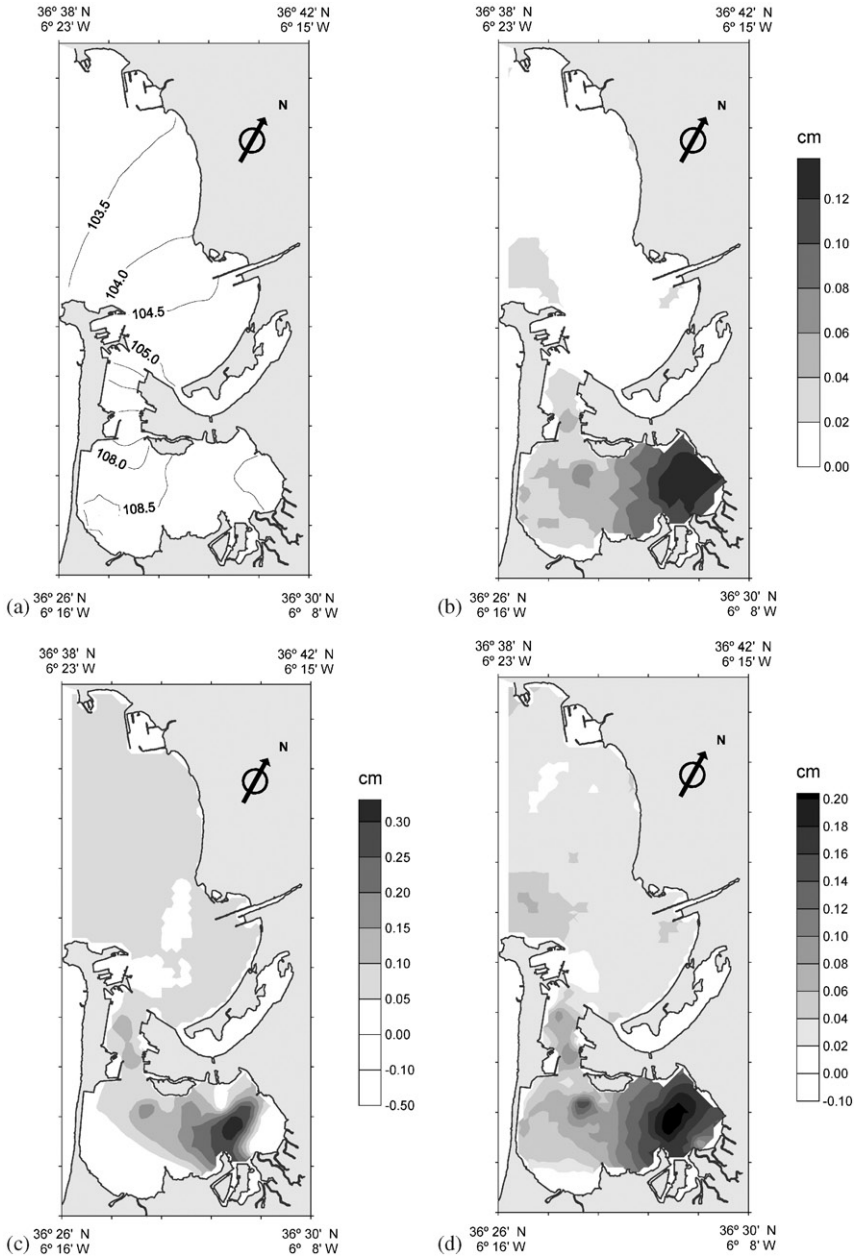

Fig. 6. Tidal elevation amplitude (in cm) (a) and its changed caused by wind-wave/tide interaction (b) and wind-wave/tide interaction and bottom mobility together (c, d). Results based on Nielsen's (1983) and Tolman's (1994) bottom roughness predictors are presented in the panels (c) and (d), respectively.

d–8c and d). So, if in Experiment 2.1 the above changes range from 0 to 1.15 N m^{-2} for the bottom stress, from −18 to 9 cm s^{-1} for the maximum depth-averaged tidal velocity, from −4.5 to 2.0 kW m^{-1} for the mean tidal energy flux per unit length, from −0.50 to 0.35 cm for the tidal elevation amplitude, from 0° to 5.5° for the tidal elevation phase, and from 0 to 0.14 W m^{-2} for the

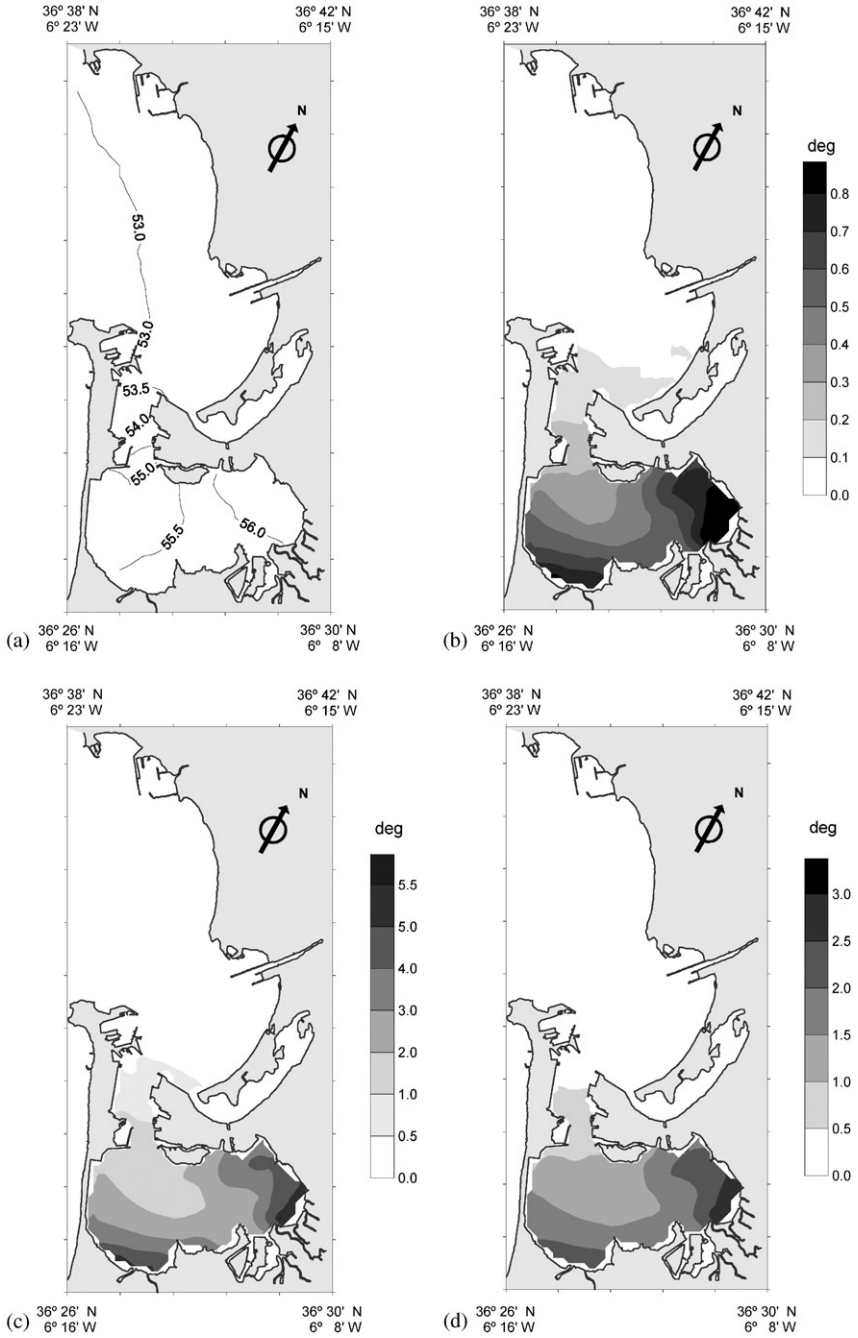

Fig. 7. Tidal elevation phase (in deg) (a) and its changes caused by wind-wave/tide interaction (b) and wind-wave/tide interaction and bottom mobility together (c, d). Results based on Nielsen's (1983) and Tolman's (1994) bottom roughness predictors are presented in the panels (c) and (d), respectively.

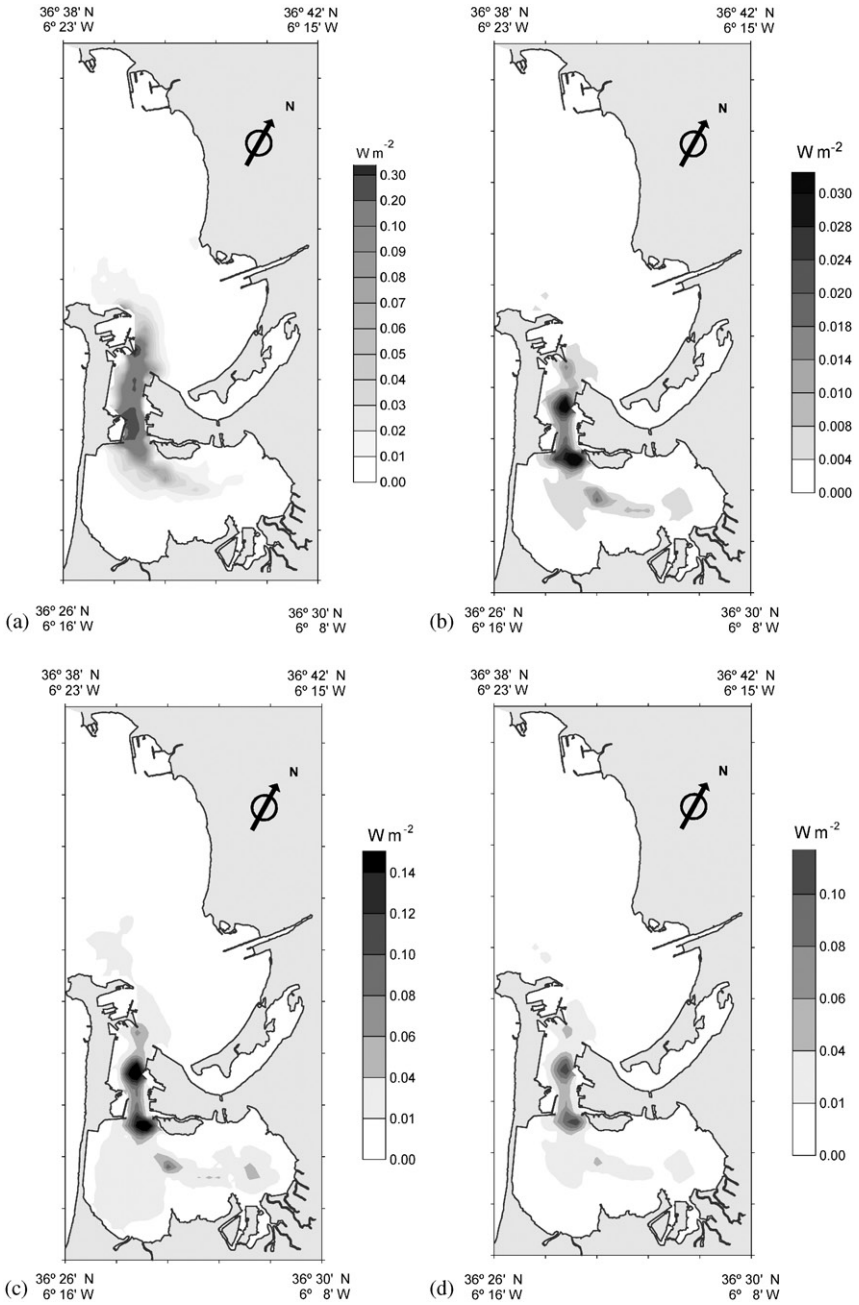

Fig. 8. Mean tidal energy dissipation (a) and its changes caused by wind-wave/tide interaction (b) and wind-wave/tide interaction and bottom mobility together (c, d). Results based on Nielsen's (1983) and Tolman's (1994) bottom roughness predictors are presented in the panels (c) and (d), respectively.

mean tidal energy dissipation, then in Experiment 2.2 their ranges are (0, 0.9) $N\,m^{-2}$, (−12, 7) $cm\,s^{-1}$, (−3.9, 1.0) $kW\,m^{-1}$, (−0.10, 0.20) cm, (0, 3.5) grad and (0, 0.15) $W\,m^{-2}$, respectively (hereinafter, the minus/plus sign is indicative of a decrease/an increase in any one characteristic relative to its

control value in Experiment 0). In short, the results show that the quantitative distinctions between Experiments 2.1 and 2.2 are not negligible.

These, however, are sufficiently small when it is considered that the values of the mobility parameter produced by Nielsen's (1983) and Tolman's (1994) bottom roughness predictors may differ by one order of magnitude or more (Fig. 9a). That is because Eqs. (1) and (6) which serve to determine the drag coefficient and the tidal bottom friction coefficient include not the mobility parameter by itself, but its product by the ratio between the wave and tidal reference bottom roughness lengths. These two multipliers are related to one another so that an increase in one of them is partially compensated for by a decrease in the other and vice versa. In addition, the logarithmic dependence of the drag coefficient on the above product is not highly sensitive to its variations. As a consequence, high values of the mobility parameter observed when employing Nielsen's (1983) bottom roughness predictor will not result in a significant increase in the drag coefficient and its related dramatic changes in the fields of tidal characteristics as compare to those provided by Tolman's (1994) bottom roughness predictor. This is encouraging.

Comparing the predicted tidal elevation amplitudes and phases with the observational data at the tide-gauge and bottom-pressure measurement locations within the bay (Table 1), we notice that a quantitative agreement between them in Experiments 2.1 and 2.2 is slightly better than in Experiment 1 and still better than in Experiment 0. It would be interesting to clarify if wind-wave/tide interaction and bottom mobility provide a better agreement with observations or not in respect to tidal current ellipse parameters. Unfortunately, appropriate empirical information is lacking in Cádiz Bay.

4.2. *Influence of wind-wave/tide interaction and bottom mobility upon the tidal energetic of Cádiz Bay*

The local values of the tidal energetic characteristics in Cádiz Bay have already been presented in the previous sub-section to better appreciate the physical mechanism for the changes in the tidal dynamics. Here we shall describe the area-averaged values of these characteristics in certain parts of the bay and the bay as a whole.

In small basins, such as Cádiz Bay, whose dimensions are much less than Earth's radius, so

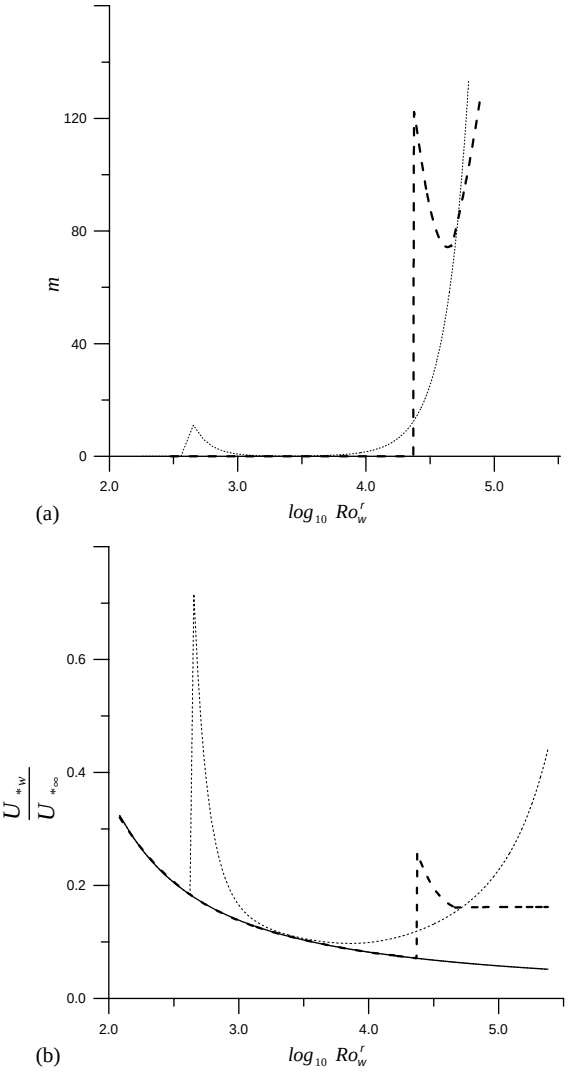

Fig. 9. Mobility parameter (a) and wave bottom friction coefficient (b) as functions of the wave surface Rossby number. The solid line in the panel (b) corresponds to the fixed rough bottom case. Results for the moveable rough bottom case obtained using Nielsen's (1983) and Tolman's (1994) bottom roughness predictors are shown by the chain and dotted lines, respectively.

Table 1
Comparison between observed and predicted tidal elevation amplitudes A and phases φ at the tide-gauge and bottom-pressure measurements locations within the bay

No.	Station	Observed		Predicted							
		A (cm)	φ (deg)	Experiment 0		Experiment 1		Experiment 2.1		Experiment 2.2	
				A (cm)	φ (deg)	A (cm)	φ (deg)	A (cm)	φ (deg)	A (cm)	φ (deg)
1.	CARRACA	108.0	60.0	109.2	56.3	108.1	56.9	108.3	59.8	108.2	57.5
2.	PTO. REAL	106.5	57.9	109.0	56.6	106.1	57.2	106.8	59.6	106.7	57.7
3.	P. CARRANZA	107.2	57.7	107.3	55.2	107.3	55.5	107.3	56.9	107.3	56.3
4.	PTO. CADIZ	103.1	55.0	104.6	53.0	103.1	53.0	103.1	53.2	103.1	53.2
5.	PTO. SHERRY	103.2	52.6	104.0	53.2	103.2	53.2	103.2	53.4	103.2	53.3
6.	ROTA	101.4	53.8	103.3	53.1	101.4	53.1	101.4	53.3	101.4	53.2

that the influence of the tide-generating force may be neglected, the mean (over a tidal cycle) area-averaged tidal energy budget is determined by the two components: (1) the mean tidal energy in-flow from and out-flow to adjacent basins and (2) the mean integral (over the region of interest) tidal energy dissipation. Since in this case both of these components must be equal in value but opposite in sign, we need only have knowledge of the changes attributable to either of them.

With this point clear, we can continue with a discussion of the changes in the mean integral tidal energy fluxes through the open boundaries of the individual parts of the bay and the bay as a whole. In the control experiment with none of wind-wave/tide interaction and bottom mobility (Experiment 0) the values of these fluxes amount to 820 kW through the open boundary of Cádiz Bay, 394 kW through the boundary between the Outer Bay and Puntales Channel and 69 kW through the boundary between Puntales Channel and the Inner Bay. The inclusion of the wind-wave/tide interaction effects (Experiment 1) is followed by an increase in the fluxes by 74, 20 and 63 kW, respectively. Concurrent allowance for the bottom mobility effects (Experiments 2.1 and 2.2) is responsible for a further increase in the fluxes by 410, 165 and 264 kW when employing Nielsen's (1983) bottom roughness predictor and by 240, 42 and 145 kW when employing Tolman's (1994) bottom roughness predictor. Curiously, it turns out that bottom mobility is every bit as important as wind-wave/tide interaction. This is due to a considerable jump-like increase and subsequent reasonably large irregular variations in the drag coefficient typical for the sediment motion evolution. It is precisely these changes in the drag coefficient that cause the mean integral tidal energy dissipation and, hence, the mean integral tidal energy fluxes to increase substantially.

4.3. Sensitivity experiments

We start with a discussion of the results of Experiments 3.1 and 3.2 on the sensitivity of the tidal dynamics of Cádiz Bay to the tidal reference bottom roughness length. The latter was assumed to be 0.1 cm, 1.0 cm (the results are not shown) and equal to the wave reference bottom roughness length, that is, in accordance with Nielsen's (1983) and Tolman's (1994) bottom roughness predictors, equal to $d/12$ and 0.03 cm, respectively, instead of 0.5 cm as specified in the foregoing experiments.

It turns out that the changes in the fields of tidal characteristics are so unreasonable that they put the very idea of prescribing the same values of the wave and tidal reference bottom roughness lengths in doubt. Indeed, the drag coefficient increases compared to its value in Experiments 2.1 and 2.2 by two or three orders of magnitude, which is accompanied by slackening tidal currents to an extent that in the Inner Bay they, in essence, disappear. Accordingly, the tidal elevation amplitudes there decrease drastically and their changes become commensurable to the tidal elevation amplitudes per se, suggesting that the sea level elevations in the Inner Bay degenerate either almost totally as in Experiment 3.1 or partially

as in Experiment 3.2. The fields of other tidal characteristics become unrecognisable as well. How significant the changes are can be inferred from Table 2 which lists the area-averaged changes in tidal characteristics in the individual parts of the bay and the bay as a whole. The appropriate changes derived in Experiments 2.1, 2.2, 4.1 and 4.2 are also presented in Table 2 for comparison. It is evident that the tidal dynamics of Cádiz Bay is highly sensitive to the tidal reference bottom roughness length.

By contrast, the variation in the mean sediment grain size from 50 μm as prescribed in Experiments 2.1 and 2.2 to 100 μm as prescribed in Experiments 4.1 and 4.2 does not lead to any qualitative changes in the fields of tidal characteristics. The quantitative changes predicted in Experiment 4.1 slightly exceed those predicted in Experiment 2.1,

Table 2
Area-averaged changes in tidal characteristics with respect to their values in the control experiment

Characteristic	Experiment					
	2.1	2.2	3.1	3.2	4.1	4.2
Inner Bay						
Drag coefficient	0.147	0.037	240	0.997	0.097	0.027
Bottom stress ($N m^{-2}$)	0.30	0.12	2.1	1.7	0.28	0.10
Maximum depth-averaged tidal velocity ($cm s^{-1}$)	−1.0	−1.2	−18.2	−5.1	−0.9	−1.5
Mean tidal energy in-flow (10^2 kW)	2.64	1.45	0.46	14.5	3.74	1.44
Tidal elevation amplitude (cm)	0.1	0.1	−100	−8	−0.1	0.1
Tidal elevation phase (deg)	2.7	1.0	110	20	3.5	1.0
Mean tidal energy dissipation ($W m^{-2}$)	0.010	0.010	0.010	0.100	0.015	0.008
Puntales channel						
Drag coefficient	0.002	0.002	26.0	0.177	0.002	0.002
Bottom stress ($N m^{-2}$)	0.60	0.23	4.50	1.90	0.45	0.21
Maximum depth-averaged tidal velocity ($cm s^{-1}$)	0.5	0.5	−4.17	2.2	0.5	0.6
Mean tidal energy in-flow (10^2 kW)	1.65	0.42	−1.32	13.52	2.76	0.40
Mean tidal energy out-flow (10^2 kW)	2.64	1.45	0.46	14.50	3.74	1.44
Tidal elevation amplitude (cm)	0.1	0.1	−70.0	-2.0	−0.1	0.1
Tidal elevation phase (deg)	1.0	0.7	60.2	5.2	1.0	0.4
Mean tidal energy dissipation ($W m^{-2}$)	0.08	0.07	0.05	0.08	0.08	0.07
Outer Bay						
Drag coefficient	0.006	0.017	32.0	0.197	0.007	0.007
Bottom stress ($N m^{-2}$)	0.08	0.08	3.60	0.30	0.05	0.06
Maximum depth-averaged tidal velocity ($cm s^{-1}$)	0.1	0.1	−8.1	−1.0	0.1	0.1
Mean tidal energy in-flow (10^2 kW)	4.10	2.40	54.18	24.48	5.98	2.39
Mean tidal energy out-flow (10^2 kW)	1.65	0.42	−1.32	13.52	2.76	0.40
Tidal elevation amplitude (cm)	0.1	0.1	−30.0	−1.0	−0.1	0.1
Tidal elevation phase (deg)	0.1	0.1	42.6	1.2	0.3	0.1
Mean tidal energy dissipation ($W m^{-2}$)	0.006	0.006	0.061	0.015	0.007	0.006
Cádiz Bay as a whole						
Drag coefficient	0.045	0.024	85.7	0.420	0.033	0.015
Bottom stress ($N m^{-2}$)	0.17	0.10	3.27	0.78	0.20	0.08
Maximum depth-averaged tidal velocity ($cm s^{-1}$)	−0.2	−0.2	−13.1	−2.2	−0.1	−0.3
Mean tidal energy in-flow (10^2 kW)	4.10	2.40	54.18	24.48	5.88	2.39
Tidal elevation amplitude (cm)	0.1	0.1	−51.0	−2.9	−0.1	0.1
Tidal elevation phase (deg)	0.9	0.4	61.4	6.4	1.2	0.4
Mean tidal energy dissipation ($W m^{-2}$)	0.012	0.011	0.050	0.043	0.019	0.021

Positive values of the changes imply an increase in the sought-for variable, negative values, a decrease.

whereas in Experiments 4.2 and 2.2 they are almost undistinguishable from each other. The reason is the distinctions between the changes in the drag coefficient in Experiments 4.1 and 4.2. In fact, if in Experiment 4.1 the drag coefficient is as great as 0.6, that is, its maximum value is about two times more than that in Experiment 2.1, then in Experiments 4.2 and 2.2 the predicted values of c_D are in close agreement. This is supported by the data of Table 2 and the following option: the changes appropriate to Experiment 4.1 range up to $2.5\,\mathrm{N\,m^{-2}}$ for the bottom stress, over $-20\,\mathrm{cm\,s^{-1}}$ for the maximum depth-averaged tidal velocity, $-5.0\,\mathrm{kW\,m^{-1}}$ for the mean tidal energy flux per unit length, $-1.5\,\mathrm{cm}$ for the tidal elevation amplitude, 9° for the tidal elevation phase and $0.25\,\mathrm{W\,m^{-2}}$ for the mean tidal energy dissipation. In Experiment 4.2 these changes are as much as $0.85\,\mathrm{N\,m^{-2}}$, $-11\,\mathrm{cm\,s^{-1}}$, $-3.5\,\mathrm{kW\,m^{-1}}$, $0.2\,\mathrm{cm}$, 2.5° and $0.15\,\mathrm{W\,m^{-2}}$, respectively. The maximum changes in tidal characteristics predicted in Experiments 2.1 and 2.2 can be easily determined from the scale bars in Figs. 3c, d–8c and d.

From the above discussion it is clear that the sensitivity of the tidal dynamics of Cádiz Bay to the mean sediment grain size is either moderate or low depending on which bottom roughness predictor, Nielsen's (1983) or Tolman's (1994), is adopted and much less than the sensitivity to the tidal reference bottom roughness length.

5. Summary and discussion

The formulation of weak wind-wave/low-frequency current interaction has been extended to the moveable rough bottom case using the bottom roughness predictors of Nielsen (1983) and Tolman (1994). This "extended" formulation is then implemented in a 2D non-linear, high-resolution hydrodynamic model and the modified model is applied to study the changes in the tidal dynamics of Cádiz Bay due to wind-wave/tide interaction and bottom mobility. The inclusion of the second of these factors is demonstrated to lead to no qualitative changes in the fields of tidal characteristics compared to those obtained with allowance for wind-wave/tide interaction alone. Certain quantitative changes, however, occur. These are such that an agreement between the predicted and observed tidal elevation amplitudes and phases tends to be improved if both of the factors are accounted for.

It has been shown that quantitative distinctions between the solutions derived when employing Nielsen's (1983) and Tolman's (1994) bottom roughness predictors are not so much as might be expected from comparison of the appropriate values of the mobility parameter. The reason for not-too-large distinctions between the two solutions is that the mobility parameter defined as the ratio of the wave-induced change in the bottom roughness length to the wave reference bottom roughness length appears in the expressions for the drag coefficient and the tidal bottom friction coefficient not by itself, but in combination with the ratio between the wave and tidal reference bottom roughness lengths. Because of this, any increase in the mobility parameter due to, say, decreasing the wave reference bottom roughness length must be partially compensated for by a decrease in the ratio between the wave and tidal reference bottom roughness lengths and vice versa.

It is for this reason that the wave and tidal reference bottom roughness lengths cannot be set equal to each other as may be inferred from the laboratory data of Mathisen and Madsen (1996a, b, 1999). Otherwise, according to the results of the numerical experiments outlined in Section 4, the solution turns out to be completely unreasonable, casting doubt upon the very idea of prescribing a single reference bottom roughness length. In fact, in this case the drag coefficient increases to an extent that the tidal elevations and velocities in the Inner Bay either almost degenerate when using Nielsen's (1983) bottom roughness predictor or are too reduced to be realistic when using Tolman's (1994) bottom roughness predictor. The fields of other tidal characteristics are also transformed beyond recognition.

Numerical experiments have been carried out to clarify the sensitivity of the solution to the tidal reference bottom roughness length and the mean sediment grain size. On varying the tidal reference bottom roughness length from 0.5 to 0.1 and 1.0 cm and comparing the obtained solutions, the

tidal dynamics of Cádiz Bay is found to be highly sensitive to the changes in this model parameter. By contrast, the sensitivity to the mean sediment grain size is either moderate or low, depending on which bottom roughness predictor, Nielsen's (1983) or Tolman's (1994), is adopted and, in any case, much less than the sensitivity to the tidal reference bottom roughness length.

From general considerations it is amply clear that the bottom roughness length is determined by the entire spectrum of roughness elements over the area with a length scale of the order of the near-bottom logarithmic layer height. Because a characteristic height of the wave BBL and, hence, a characteristic height of the wave near-bottom logarithmic layer are much less than their tidal counterparts, the wave and tidal reference bottom roughness lengths must widely differ in magnitude. If so, why do the laboratory data of Mathisen and Madsen (1996a, b, 1999) provide a single bottom roughness length?

To answer this question, let us recall that Mathisen and Madsen (1996a, b, 1999) made use of different techniques to evaluate the current and wave bottom roughness lengths; more specifically, the first of these lengths was determined from time-averaged velocity profiles in the current near-bottom logarithmic layer, while the second, from measurements of wave attenuation. The length scale on which the process of wave attenuation operates, however, is of the order of the wave length, that is, is much superior to the characteristic height of the wave near-bottom logarithmic layer. Moreover, the height of and spacing between roughness elements were taken invariant within the wave flume, so that it is hardly surprising that the wave and current bottom roughness lengths have close values in laboratory conditions. The opposite situation is apparently the rule than the exception in field conditions. The above-mentioned numerical experiments with the same values of the wave and tidal reference bottom roughness lengths may be regarded as an additional argument in favour of this conclusion.

However, if for wave-affected tidal flows the use of different values of the wave and tidal reference bottom roughness lengths appears to be justified, then for the pure wave case this is in principle impossible. In this case, the only way of lowering the excessive sensitivity to the bottom roughness length is to increase its value. It is this way that was applied by Tolman (1994) who first defined the wave reference bottom roughness length as a background ("base") roughness length related to relict roughness elements. As evident from Fig. 9, a lowering of the sensitivity is accomplished thus: by decreasing the mobility parameter which, by definition, is decreased as the wave reference bottom roughness length increases and by increasing the "background" wave bottom friction coefficient from which its bottom mobility-induced changes are reckoned. An increase in the "background" wave bottom friction coefficient, in turn, is attended with the shift of all sediment motion regimes into the range smaller values of the wave surface Rossby number complying with greater values of the wave bottom friction coefficient.

Notice that the wave bottom friction coefficient is a discontinuous function of the wave surface Rossby number. This feature is determined by initial ripple formation and is responsible for maintenance of a strong sensitivity of the wave field to sediment parameters. To avoid its unwanted consequences, Tolman (1995) and Ardhuin et al. (2001) proposed to account for the spatial variability of the bottom roughness length on subgrid scales, assuming that the parameters determining bottom mobility are stochastic variables with known statistical properties. For lack of required information, this suggestion is still unused in field conditions. But even if this information were available, the wave reference bottom roughness length could not be increased far beyond 0.03 cm adopted by Tolman (1994). Otherwise, the roughness elements corresponding to an increased wave reference bottom roughness length ought to be reproduced explicitly (and not implicitly in terms of the roughness length) as having the length scale exceeding the characteristic height of the wave near-bottom logarithmic layer.

Another point that should be mentioned especially is that the solution of the time-periodic boundary problem employed by Grant and Madsen (1982) to obtain the resistance law for an oscillatory rough BBL is valid only for heights ranging from the bottom roughness length (the

wave reference bottom roughness length in the pure wave case) to the top of the BBL. Meanwhile, the solution is applied to evaluate the skin friction velocity amplitude at the sediment grain roughness length, the length that is much less than the background bottom roughness length in Tolman's (1994) bottom roughness predictor. In other words, the solution is extrapolated beyond the domain of its determination. The same shortcoming is inherent in our formulation of weak wind-wave/tide interaction when coupled with Tolman's (1994) bottom roughness predictor. The implementation of Nielsen's (1983) bottom roughness predictor eliminates this defect, but, as noted above, gives rise to unrealistically large changes in the fields of the sought-for characteristics.

The last point we would like to dwell on concerns the quasi-monochromatic approximation of the wave field. At first sight it seems that, because the near-bottom wave orbital velocity has a narrow spectrum with no high-frequency components, this approximation holds good. At small depths and/or strong wind velocities, however, when the near-bottom wave orbital velocity spectrum is broad enough, the possibility of the quasi-monochromatic approximation being used is not evident. It is not also clear yet how to resolve the dilemma just mentioned and what errors are introduced by the extrapolation of the solution beyond its range of validity. What is clear is that these outstanding questions as well as the mere problem of wave–tide–sediment interaction deserve more attention than has been accorded to them up to now.

Acknowledgements

The work was carried out during a stay of B.A. Kagan as visiting scientist at University of Cádiz and was partially supported by the DC-type grant of the NATO Scientific Committee, the NATO Linkage grant EST.CLG 975279, and the Russian Basic Research Foundation grant 01-05-64981. We appreciate the numerous valuable suggestions on our manuscript by Dr. Alan M. Davies and an anonymous reviewer.

References

Aldridge, J.N., Davies, A.M., 1993. A high-resolution three-dimensional hydrodynamic tidal model of the eastern Irish Sea. Journal of Physical Oceanography 23, 207–224.

Álvarez, O., Tejedor, B., Tejedor, L., 1997. Simulación hidrodinámica en al área de la Bahía de Cádiz. Análisis de las constituyentes principales. In: IV Jornadas Españolas de Puertos y Costas. Servicio de Publicaciones de la Universidad Politécnica de Valencia-98, Vol. 2125, pp. 125–136.

Álvarez, O., Izquierdo, A., Tejedor, B., Mañanes, R., Tejedor, L., Kagan, B.A., 1999. The influence of sediment load on tidal dynamics a case study: Cádiz Bay. Estuarine Coastal and Shelf Sciences 48, 439–450.

Ardhuin, F., Herbers, T.H.C., O'Reeilly, W.C., 2001. A hybrid-Eulerian–Lagrangian model for spectral wave evolution with application to bottom friction on the continental shelf. Journal of Physical Oceanography 31, 1498–1516.

Christofferesen, J.B., Jonsson, I.G., 1985. Bed friction and dissipation in a combined current and wave motion. Ocean Engineering 12, 387–423.

Davies, A.M., Jones, J.E., 1996. The influence of wind and wind-wave turbulence upon tidal currents: Taylor's problem in three dimensions with wind forcing. Continental Shelf Research 16, 25–99.

Davies, A.M., Lawrence, J., 1994. Examining the influence of wind and wind wave turbulence on tidal currents using a three dimensional hydrodynamic model including wave–current interaction. Journal of Physical Oceanography 23, 2441–2460.

Davies, A.M., Lawrence, J., 1995. Modelling the effect of wave–current interaction on the three-dimensional wind driven circulation of the eastern Irish Sea. Journal of Physical Oceanography 25, 29–45.

Dietrich, W.D., 1982. Flow, boundary shear stress and sediment transport in a river meander. Ph.D. Dissertation, University of Washington, p. 261.

Graber, H.C., Madsen, O.S., 1988. A finite-depth wind-wave model Part 1: model description. Journal of Physical Oceanography 18, 1465–1483.

Grant, W.D., Madsen, O.S., 1979. Combined wave and current interaction with a rough bottom. Journal of Geophysical Research 84, 1797–1808.

Grant, W.D., Madsen, O.S., 1982. Movable bed roughness in unsteady oscillatory flow. Journal of Geophysical Research 87, 469–481.

Grant, W.D., Williams, A.Y., Glenn, S.M., 1984. Bottom stress estimates and their prediction on the northern California continental shelf during CODE-1: the importance of wave–current interaction. Journal of Physical Oceanography 14, 506–527.

Gutiérrez, J.M., Achab, M., Parado, J.M., 1996. Distribution of recent facies at the bottom of the Bay of Cádiz. Geogaceta 21, 155–157.

Heathershaw, A.D., 1981. Comparison of measured and predicted sediment transport rates in tidal currents. Marine Geology 42, 75–104.

Johnson, H.K., Kofoed-Hansen, H., 2000. Influence of bottom friction on sea surface roughness and its impact on shallow water wind wave modeling. Journal of Physical Oceanography 30, 1743–1756.

Kagan, B.A., Utkin, K.B., 2000. Weak wave–tide interaction and the drag coefficient in a tidal flow. Izvestiya Atmospheric and Oceanic Physics 36, 566–574.

Kagan, B.A., Tejedor, L., Álvarez, O., Izquierdo, A., Tejedor, B., Mañanes, R., 2001. Weak wave–tide interaction formulation and its application to Cádiz Bay. Continental Shelf Research 21, 697–725.

Kagan, B.A., Alvarez, O., Izquierdo, A., Mananes, R., Tejedor, B., Tejedor, L., 2003. Weak wave/tide interaction in suspended sediment-stratified flow: a case study. Estuarine, Coastal and Shelf Sciences 56, 1–12.

Li, M.Z., Amos, C.L., 1998. Predicting ripple geometry and bed roughness under combined waves and currents in a continental shelf environment. Continental Shelf Research 18, 941–970.

Longuet-Higgins, M.S., 1969. On wave breaking and the equilibrium spectrum of wind-generated waves. Proceedings of the Royal Society, London, A 310, 151–159.

Madsen, O.S., Mathiesen, P.P., Rosengaus, M.M., 1990. Movable bed friction factors for spectral waves. Proceedings of the 22nd International Conference on Coastal Engineering. ASCE, Delft, pp. 420–429.

Mathisen, P.P., Madsen, O.S., 1996a. Waves and currents over a fixed rippled bed. 1. Bottom roughness experienced by waves in the presence and absence of currents. Journal of Geophysical Research 101, 16533–16542.

Mathisen, P.P., Madsen, O.S., 1996b. Waves and currents over a fixed rippled bed. 2. Bottom and apparent roughness experienced by currents in the presence of waves. Journal of Geophysical Research 101, 16543–16550.

Mathisen, P.P., Madsen, O.S., 1999. Waves and currents over a fixed rippled bed. 3. Bottom and apparent roughness for spectral waves and currents. Journal of Geophysical Research 104, 18447–18461.

Nielsen, P., 1983. Analytical determination of near-shore wave height variation due to refraction shoaling and friction. Coastal Engineering 7, 233–251.

Signell, R.P., Berdsley, R.C., Graber, H.C., Capotondi, A., 1990. Effect of wave–current interaction on wind-driven circulation in narrow, shallow embayment. Journal of Geophysical Research 95, 9671–9678.

Tang, Y.M., Grimshaw, R., 1996. The effect of wind-wave enhancement of bottom stress on the circulation induced by tropical cyclones on continental shelves. Journal of Geophysical Research 101, 22705–22714.

Tejedor, L., Tejedor, B., Álvarez, O., Izquierdo, A., Vidal, J., 1998. Modelo de evaluación técnica para la gestión y ordenación de estuarios. Technical Report, Departamento de Física Aplicada, Universidad de Cádiz, Cádiz, Spain, 150pp, unpublished.

Tolman, H.L., 1994. Wind waves and movable-bed bottom friction. Journal of Physical Oceanography 24, 994–1009.

Tolman, H.L., 1995. Subgrid modelling of moveable-bed bottom friction in wind wave models. Coastal Engineering 26, 57–75.

Wiberg, P.L., Rubin, D.M., 1989. Bed roughness produced by saltating sediment. Journal of Geophysical Research 94, 5011–5016.

Young, I.R., Gorman, R.M., 1995. Measurements of the evolution of ocean wave spectra due to bottom friction. Journal of Geophysical Research 100, 10987–11004.